

## Flow and Hydraulics near the Sill of Hood Canal, a Strongly Sheared, Continuously Stratified Fjord

M. C. GREGG

*Applied Physics Laboratory, University of Washington, Seattle, Washington*

L. J. PRATT

*Woods Hole Oceanographic Institution, Woods Hole, Massachusetts*

(Manuscript received 13 July 2009, in final form 29 December 2009)

### ABSTRACT

Hood Canal, a long fjord in Washington State, has strong tides but limited deep-water renewal landward of a complex constriction. Tide-resolving hydrographic and velocity observations at the constriction, with a depth-cycling towed body, varied markedly during three consecutive years, partly because of stratification variations. To determine whether hydraulic control is generally important and to interpret observations of lee waves, blocking, and other features, hydraulic criticality is estimated over full tidal cycles for channel wide internal wave modes 1, 2, and 3, at five cross-channel sections, using mode speeds from the extended Taylor–Goldstein equation. These modes were strongly supercritical during most of ebb and flood on the gentle seaward sill face and for part of flood at the base of the steep landward side. Examining local criticality along the thalweg found repeated changes between mode 1 being critical and supercritical approaching the sill crest during flood, unsurprising given local minima and maxima in the cross-sectional area, with the sill crest near a maximum. Density crossing the sill sometimes resembled an overflow with an internal hydraulic control at the sill, followed by a hydraulic jump or lee wave. Long-wave speeds, however, suggest cross waves, particularly along the shallower gentler side, where flow downstream of a large-amplitude wave was uniformly supercritical. Supercritical approaching the sill, peak ebb was critical to mode 1 and supercritical to modes 2 and 3 at the base while forming a sluggish dome of dense water over the sill. Full interpretation exceeds observations and existing theory.

### 1. Introduction

Hood Canal, a fjord in Washington State lying at the base of the Olympic Mountains (Fig. 1), attracts a growing population, increasing environmental stress, and public concern. A long sill at the northern end of the canal limits exchanges of dense water between the deeper southern reach and Admiralty Inlet, the channel linking Puget Sound to the North Pacific Ocean via the Strait of Juan de Fuca. Renewals of the deep water are most likely during autumn, when upwelling offshore brings in more saline water, displacing bottom water beyond the sill and increasing the oxygen content of the canal's southern reach. After these renewals, oxygen concentrations south of the sill steadily decrease to hypoxic conditions,

defined as concentrations of dissolved oxygen less than  $3 \text{ mL L}^{-1}$ , sometimes accompanied by fish kills and public alarm (Newton et al. 2007).

Because understanding hydraulic control of flows over the sill is central to predicting and modeling renewals of the hypoxic water in the southern reach, Washington Sea Grant funded a detailed observational program with a depth-cycling towed body during 2001, 2002, and 2003. Bathymetry and data collection are summarized in section 2, followed in section 3 by a brief review of long-wave and hydraulic theory applicable to Hood Canal. The main features of the flow and stratification are presented in section 4 along with estimates of hydraulic control. Conclusions are summarized and discussed in section 5. A future paper will examine energy fluxes and mixing.

### 2. Bathymetry and observations

Beginning at the seaward end of Hood Canal, distances along the thalweg, or deepest path, reference our

---

*Corresponding author address:* M. C. Gregg, Applied Physics Lab., University of Washington, 1013 NE 40th St., Seattle, WA 98105.  
E-mail: gregg@apl.washington.edu

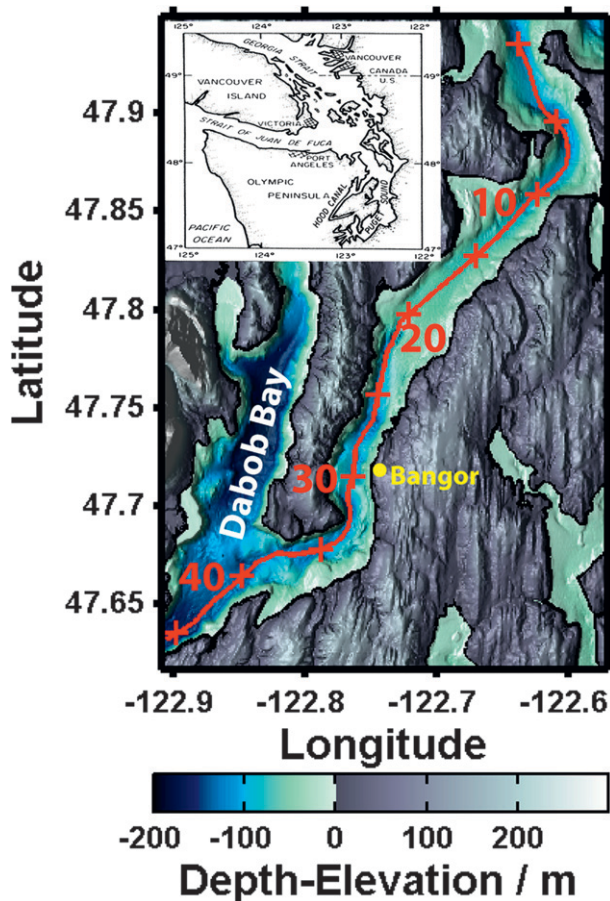


FIG. 1. Northern half of Hood Canal, from the junction with Admiralty Inlet in the north to Dabob Bay, with an insert showing the relation of the fjord to Admiralty Inlet and Puget Sound. The thalweg is red, marked at 5-km intervals from 47°56.124'N, 122°38.286'W. From a local deep near 5 km, the sill rises steadily to a crest at 20 km, followed by a steep drop on the west side of the channel and a gradual descent along the east side.

observations to the bathymetry (Fig. 1). Changes in width and depth produce multiple local extrema in cross-sectional area (Fig. 2). Unlike typical situations, the crest, or shallowest part of the thalweg at 20 km, does not coincide with a minimum in area. Rather, in this part of the channel the minimum in area (i.e., the choke) is at 16 km, slightly landward of cross-channel section x1 (Fig. 3). Three or four secondary minima occur between 20 and 28 km.

Widening dominates changes in area landward of the choke at 15.5 km, leading to an area maximum near 21 km, 1 km past the crest. Along the thalweg, the crest lies in a hanging valley on the west side of the channel; the east side slopes gradually downward toward the south, steadily thinning until disappearing near 26 km (Fig. 3). South of the sill, the bottom along the thalweg is very rough, varying by  $\pm 25$  m over 1 km or less. After a

constriction at 32 km, the channel turns sharply clockwise toward the mouth of Dabob Bay, a small secondary fjord extending northward from the canal. Because of flow separations, stream tube areas may differ from those of the channel, but we lack information to evaluate this, except where we took cross-channel runs.

Several rivers flowing down from the Olympics enter the western side of the canal between the northern end of Dabob Bay and the Great Bend near the southern end. Fed by rain and melting snow, these rivers usually peak between late spring and midsummer.

All measurements were with the Shallow Water Integrated Mapping System (SWIMS), a depth-cycling body, towed at 4–6 kt by the R/V *Miller*, a 50-ft vessel capable of working in shallow water. SWIMS1, used during 2001, carried a Sea-Bird 9/11 CTD with duplicate temperature and conductivity probes. Currents were measured with an RD Instruments 300-kHz Workhorse Sentinel mounted on the *Miller*. SWIMS2, used during 2002 and 2003, had a 911+ Sea-Bird CTD with additional channels including dissolved oxygen, a fluorometer with a chlorophyll filter, and optical backscatter that detected suspended particles. In addition, SWIMS2 had upward and downward 300-kHz ADCPs. To avoid interference with these ADCPs, the vessel-mounted ADCP on the *Miller* was changed to a 150-kHz broadband unit during 2002 and 2003. Acoustic altimeters allowed SWIMS to come routinely within a few meters of the bottom. Upward legs turned around at 5 m to avoid fouling the conductivity probes with bubbles from the vessel's propeller. High-frequency BioSonics acoustic backscatter systems, at 120 and 208 kHz, supplemented all observations.

Because the *Miller* lacked bunks, observations were limited to one tidal period of nominally 12.5 h, typically from slack preceding a major ebb to slack after the next flood. Table 1 gives the times of the observations, and Fig. 4 relates them to tidal phase. Times are in yeardays, elapsed UTC days during the year beginning at 0.0 at midnight of the previous year. Successive transects along a waypoint set are collected into groups, and individual transects are termed subs. Work began on 6 April 2001, close to spring tides, along x1, crossing the thalweg at 14.9 km, 5 km seaward of the sill crest (Fig. 3). We completed 19.5 crossings during the tidal cycle. The next day, x2 and x3 were run in tandem, resulting in 10 loops around the combined track. Two days later, thalweg transit th1 consisted of 10 transits back and forth along the thalweg between 14.5 and 23 km, crossing the sill each time.

Beginning 10 days later in the season, the 2002 runs started with several thalweg transits (th2) between 15 and 25 km to observe along-channel structures being advected back and forth across the sill by the tides. The next day, tandem x4 and x5 were run south of the sill,

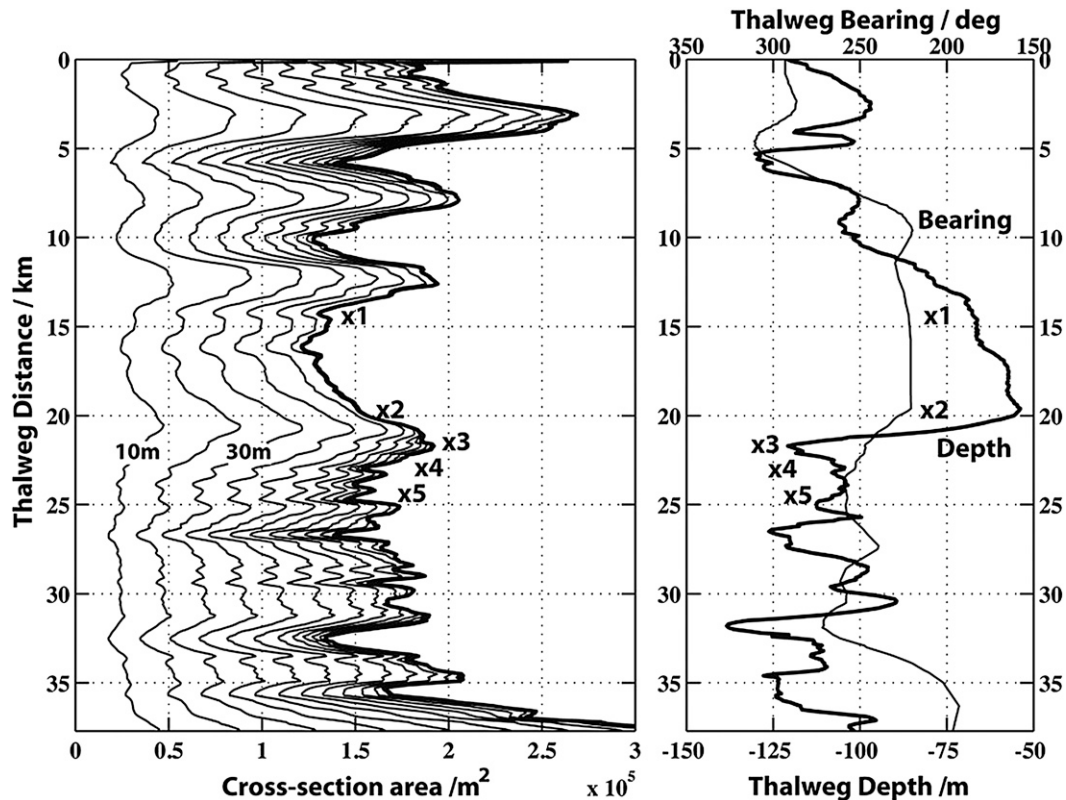


FIG. 2. (left) Cross-sectional area of Hood Canal from Admiralty Inlet to Dabob Bay. Thin lines are cumulative area ( $\text{m}^2$ ) upward from the bottom at 10-m intervals; the thick line is the total area. Local minima and maxima occur at 5–10-km intervals along the thalweg. By a slight margin, the area minimum at 15.5 km is the smallest in the northern half of the canal; x1–x5 are locations of SWIMS cross-channel runs. (right) Thalweg depth (m) and bearing ( $^\circ$ ) going landward. Note that the minimum depth, at the sill crest, does not coincide with an area minimum area but is close to a maximum.

obtaining 13 runs along x4 and 14 runs along x5. Two days later, th3 consisted of 19 thalweg runs over the sill crest between 18.9 and 23.6 km. Finally, S1 followed a streamline over the more gentle eastern side of the sill.

The 2003 observations began on 26 October with a grid pattern (not shown in Fig. 3) over the eastern shelf. These were followed with S2, slightly east of S1; th4, from 25 to 35 km, concluded the observations by examining flow 5 km landward of the sill crest, designated th4, along a region of large bumps on the bottom.

### 3. Long waves and hydraulics

A complete description of the hydraulic properties of Hood Canal is hindered by complex geometry, time dependence, and the lack of distinct interfaces in velocity and stratification, precluding application of hydraulic theory developed for layered flow. Although these features impede direct comparison with idealized models of hydraulics and lee waves, it is of interest to compute the observed parameters that characterize these

models. For example, consider the flow set up when a hydrostatic, two-dimensional, stratified flow of constant depth  $D$ , constant buoyancy frequency  $N$ , and constant velocity  $U$  encounters an isolated obstacle of height  $h$ . As summarized in Baines (1995), the adjusted state is governed by two nondimensional parameters  $Nh/U$  and  $ND/\pi U$ . The former is a measure of the obstacle height, and the latter is an inverse Froude number. Both are based on the initial values of  $N$  and  $U$ , the meaning of which is uncertain in the present context. Also, calculation of an unambiguous  $h$  from the thalweg depth (Fig. 2) is difficult; however, if we take  $h = 60$  m as a characteristic height difference along the thalweg and use peak tide values (in the deeper reaches) of  $U \approx 0.4 \text{ m s}^{-1}$  and  $N \approx 8 \times 10^{-2} \text{ s}^{-1}$ , then  $Nh/U$  is close to unity. In the idealized experiments, this would indicate that  $h$  is sufficiently large to create dramatic processes such as upstream blocking of dense water, lee separation, and static instability of internal lee waves. For these values and  $D = 100$  m,  $ND/\pi U = 0.6$ , implying that flow approaching the sill is supercritical, a property that seems to be verified

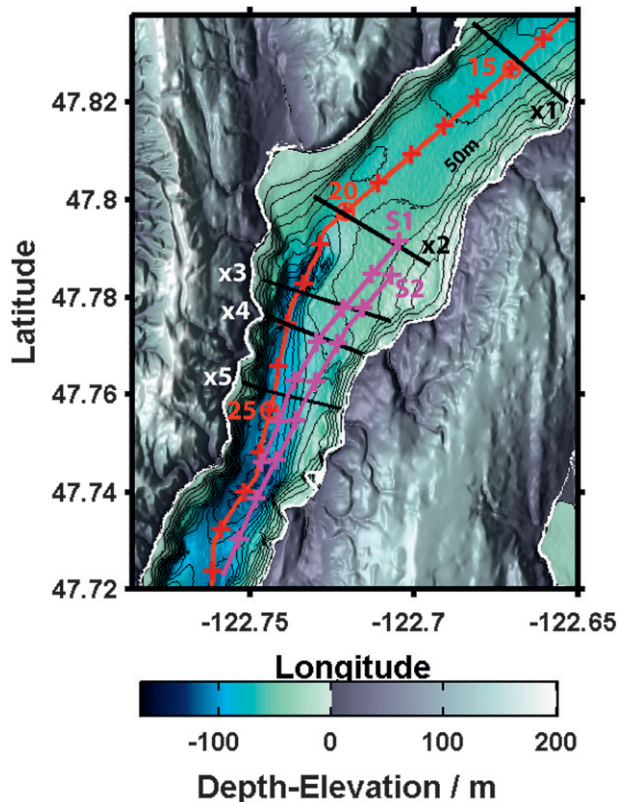


FIG. 3. Detail of the sill overlaid with sampling tracks and isobaths at 10-m intervals. Southward of the sill crest at 20 km, the bottom on the western side drops off steeply, while the eastern side slopes more gently downward. Black lines are x1–x5, from north to south; x1, x2, and x3 were run during 2001, and x4 and x5 were run during 2002. Maroon lines S1 (2002) and S2 (2003) follow streamlines.

by the more ambitious calculations described later. Supercritical approach flow would appear to have interesting hydraulic implications; however, pictures suggested by these parameter values are clouded, among other things,

by the complex variation of the cross-sectional shape. For example, x1, across the sill crest, is not at a minimum in cross-sectional area (Fig. 2); to the contrary, it is only a few hundred meters seaward of an area maximum.

To gain an improved quantification of the hydraulic character of the flow, we have attempted to assess its criticality, section by section, in a way that takes into account variations in the width and shape of the channel and that also accounts for nonuniform vertical variations in the velocity and stratification. We do so by directly estimating the speed of the long internal wave modes of the flow at a number of sections. This calculation considers local channel shape and uses as cross-channel average profiles of velocity  $U(z)$  and buoyancy frequency  $N(z)$ . The resulting dynamical modes are solutions to the extended Taylor–Goldstein equation (Pratt et al. 2000),

$$(U - c) \frac{d^2 \bar{w}}{dz^2} + \left( \frac{N^2}{U - c} - \frac{d^2 U}{dz^2} \right) \bar{w} + \frac{d}{dz} [(U - c) T \bar{w}] = 0, \quad (1)$$

where the eigenvalue  $c$  is the phase speed and the corresponding eigenfunction  $\bar{w}(z)$  gives the structure of the associated vertical wave velocity. The shape of the channel at the cross section in question is contained in

$$T(z) = b^{-1} db/dz, \quad (2)$$

where  $b(z)$  is the channel width at given elevation  $z$  above bottom. Surface and bottom boundary conditions are

$$\bar{w}(0) = \bar{w}(D) = 0, \quad (3)$$

where  $z = -D$  is at the depth maximum for the section.

TABLE 1. Observations in Hood Canal. Yearday begins as 0.0 at midnight 31 Dec of the preceding year. Group and sub numbers link runs to our database. Groups are sets of similar runs (e.g., comprising x1), and subs are indexes of sequential runs during a group. Sub 8 of th4 was run across channel at 35 km.

Name	Year	Yearday	Cruise	Group	Subs	Location
x1	2001	95.4836–95.9767	ps01	2	20	Cross section at 14.8 km
x2	2001	96.5102–96.9895	ps01	3	10	Cross section at 20.0 km (Sill Crest)
x3	2001	96.5323–97.0140	ps01	4	10	Cross section at 22.2 km
th1	2001	98.5679–99.0846	ps01	5	10	Along thalweg 4.1–25.1 km
th2	2002	114.7187–114.9405	ps02	1	3	Along thalweg 16–26 km
x4	2002	115.4928–116.0044	ps02	2	14	Cross section at 23.0 km
x5	2002	115.5100–115.9858	ps03	3	13	Cross section at 24.5 km
th3	2002	117.5184–118.0606	ps02	4	19	Along thalweg 18.5–22.6 km
S1	2002	118.5439–119.0849	ps02	5	15	Streamline east of sill crest
Grid2	2003	298.0294–298.5512	hc03	1–8	1–6	Grid east of sill crest
S2	2003	299.0881–299.6175	hc03	9	11	Streamline east of sill crest
th4	2003	301.1062–301.6027	hc03	11	9	Along thalweg 25.0–35.0 km

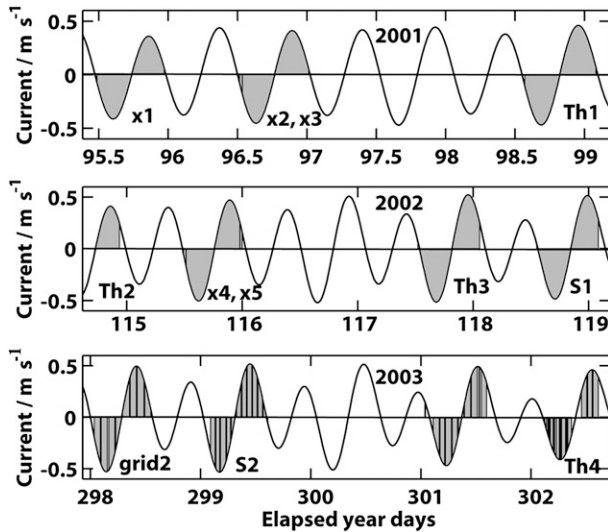


FIG. 4. Barotropic tidal currents near the sill from the National Oceanic and Atmospheric Administration tidal model of Puget Sound. Landward currents ( $\text{m s}^{-1}$ ) are positive, and times of SWIMS sampling are shaded. During 2001, x2 and x3 were run the same day as the cross-channel legs of a clockwise loop; x4 and x5 were executed in a similar manner during 2002. Vertical lines during 2003 show times of subs, successive runs, along the same waypoints. Elapsed year days began as 0.0 at midnight on 31 Dec of the previous year.

Eigenfunctions, normalized  $\overline{w(z)}_i$ , and eigenvalues  $c_i$  of (2) and (3) are restricted by theorems developed by Deng et al. (2003). A particularly useful result specifies the ordering of eigenfunctions and bounds on their values, provided that the minimum value of the Richardson number  $\text{Ri} \equiv N^2/(dU/dz)^2$  does not fall beneath  $1/4$  over the water column. In this case, there exists an infinite number of neutral discrete eigenvalues  $c_1, c_2, \dots$ , such that

$$\begin{aligned}
 U_{\min} - \frac{N_{\max} D}{[\pi^2 + 1/4(T_{\min}^2 D^2)]^{1/2}} &< c_{-1} < c_{-2} < c_{-3} \dots \\
 &< U_{\min} \leq U_{\max} < \dots < c_3 < c_2 < c_1 < U_{\max} \\
 &+ \frac{N_{\max} D}{[\pi^2 + 1/4(T_{\min}^2 D^2)]^{1/2}}. \tag{4}
 \end{aligned}$$

In other words, the long-wave modes occur in pairs, with pair  $j$  having speeds  $c_{-j}$  and  $c_j$  ( $j \geq 1$ ). For a given  $j$ , each member of the pair has exactly  $j - 1$  zero crossings. Thus,  $j = 1$  corresponds to a pair of waves having phase speeds  $c_{-1}$  and  $c_1$ , each of which has no zero crossings in its  $\overline{w(z)}$  profile. They are the first baroclinic modes. The wave speeds for all modes lie outside the range  $U_{\min} \leq U \leq U_{\max}$  of the basic velocity but within a finite factor  $N_{\max} D / [\pi^2 + 1/4(T_{\min}^2 D^2)]^{1/2}$  of the velocity extremes. For a given  $j$ ,  $c_{-j}$  and  $c_j$  lie on either side of the velocity

extremes, with the first-mode speeds lying furthest away. As  $j$  increases, the modes acquire more zero crossings, and their speeds move in toward the extremes of  $U(z)$ .

Hydraulic control with respect to a particular  $j$  occurs when either  $c_{-j}$  or  $c_j$  is zero. In this case, we say that the flow is hydraulically critical with respect to  $j$ . In consideration of the uncertainty in calculating the speeds from data, we will use the term critical to describe any circumstance in which the magnitude of  $c_{-j}$  or  $c_j$  is less than  $0.05 \text{ m s}^{-1}$ . If this condition does not hold and  $c_{-j}c_j < 0$  (the two waves propagate in opposite directions), we call the flow subcritical with respect to  $j$ . Supercritical flow occurs when the two modes propagate in the same direction  $c_{-j}c_j > 0$ .

If  $\text{Ri}$  falls below  $1/4$  for some  $z$  range, the discrete modes may no longer be infinite in number, and some may be unstable; in extreme cases, there may be no discrete modes. In most of the cases considered,  $\text{Ri}_{\min}$  does indeed fall below  $1/4$ , however, in all such cases, we still find neutrally stable first, second, and third modes having phase speeds that obey the bounds and ordering described earlier. Overtorns in some vertical profiles indicate the presence of shear instabilities, but these occur in higher vertical modes, ones whose vertical structures are difficult to resolve in our calculations.

Solutions to (1) and (2) were computed numerically at x1–x5 using a finite difference code descended from a program originally developed by Winters and Riley (1992). Examples of the vertical structure of the first three modes at x2 for peak ebb and peak flood (Fig. 5) reveal behavior quite different from more familiar baroclinic modes in shearless flows. The left-hand panels show the averaged  $U$  and  $N^2$  profiles while the remaining panels show the vertical structures corresponding to  $j = -1, -2$ , and  $-3$  (middle) and  $j = 1, 2, 3$  (right). We call the former group seaward modes because they propagate seaward in the absence of a current; the latter are landward. As shown in the middle panel,  $j = -1$  has no zero crossings, while  $j = -2$  has one, and  $j = -3$  has two. The fact that all zero crossings occur in the upper portion of the water column is suggested by the following argument: Disregarding the effects of topography, (1) can be rewritten as

$$\frac{d^2 \overline{w}}{dz^2} + \left[ \frac{N^2}{(U - c)^2} - \frac{1}{(U - c)} \frac{d^2 U}{dz^2} \right] \overline{w} = 0, \tag{5}$$

suggesting that the local vertical wavenumber is  $[N^2 / (U - c)^2 - 1 / (U - c) d^2 U / dz^2]^{1/2}$ . As  $j$  increases,  $c_{-j} \rightarrow U_{\min}$  from below [see Eq. (4)]; thus, the quantity  $N^2 / (U - c)^2$  increases in magnitude near the top of the water column, where  $U = U_{\min}$ . Thus, the eigenfunction might be expected to wiggle most rapidly in the upper water column.

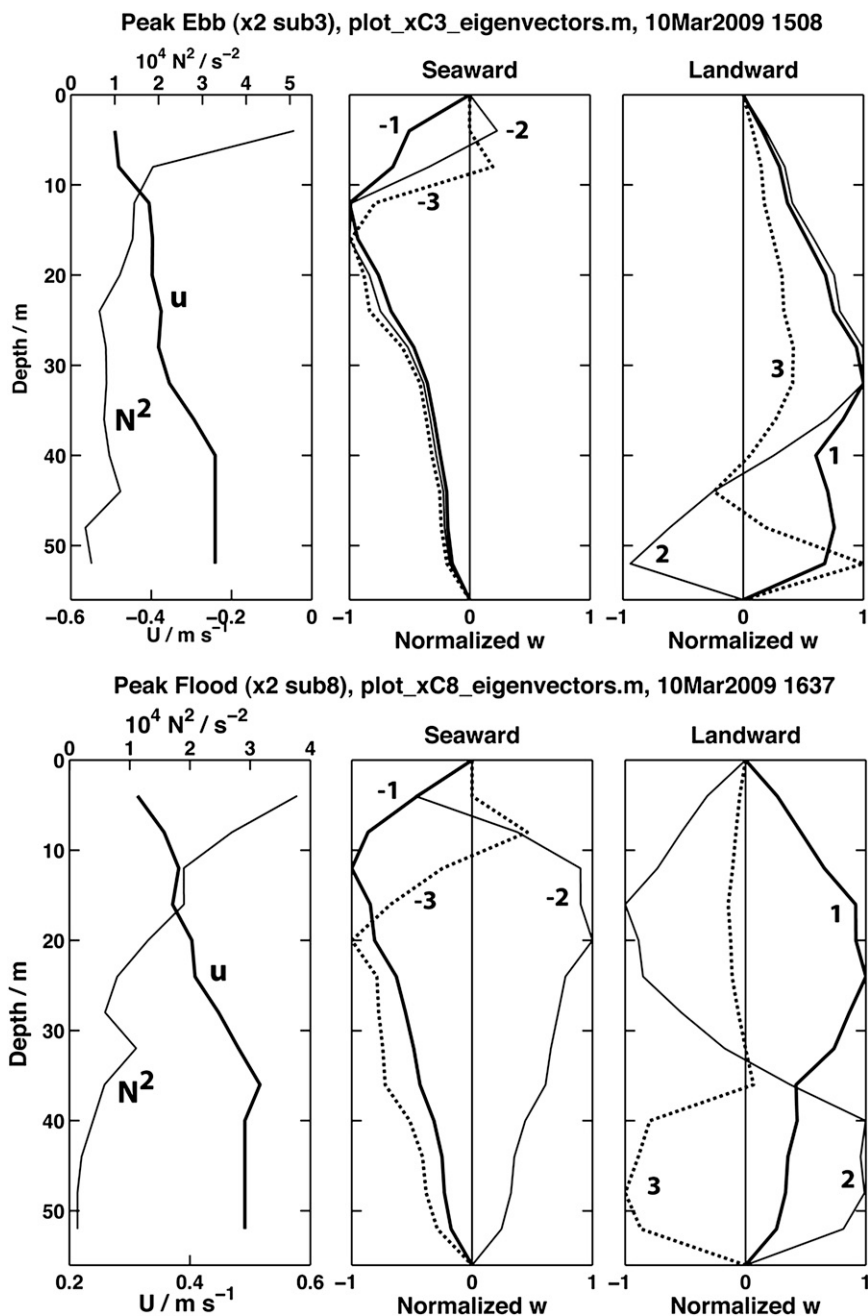


FIG. 5. Normalized vertical velocities, eigenfunctions, at the sill crest during (top) peak ebb and (bottom) peak flood, obtained by solving (1) with along-channel velocity and  $N^2$  averaged across x2 (2001). (middle), (right) Modes propagating seaward and landward are shown. Wave speeds and eigenvalues, (top) x2 sub 3 (2001) are  $-0.590$  and  $-0.177$   $\text{m s}^{-1}$  (mode 1);  $-0.538$  and  $-0.209$   $\text{m s}^{-1}$  (mode 2); and  $-0.498$  and  $-0.217$   $\text{m s}^{-1}$  (mode 3) and (bottom) x2 sub 8 (2001) are  $+0.204$  and  $+0.574$   $\text{m s}^{-1}$  (mode 1);  $0.274$  and  $0.531$   $\text{m s}^{-1}$  (mode 2); and  $0.312$  and  $0.523$   $\text{m s}^{-1}$  (mode 3). Having the same signs, all modes are supercritical.

The same argument suggests that the landward modes ( $j = 1, 2, 3$ ) should have zero crossings near the bottom, because  $U_{\min}$  occurs there, and this is consistent with what is shown in the right-hand panels (Fig. 5). Similar properties hold at peak flood, where  $U_{\min}$  lies at the surface and  $U_{\max}$  is approximately two-thirds down through the water column. The concentration of the zero crossings near the velocity extremes makes it difficult to distinguish between the modes: the eigenfunctions may look similar over most of the water column and are distinguished only after one counts zero crossings compressed into a small depth range. It is doubtful that our calculations, which are typically based on 15–20 vertical bins of data, are able to distinguish anything beyond the third vertical mode.

This discussion pertains to wave modes that fill a channel cross section and satisfy boundary conditions implied by the vanishing of depth at the edges. These are the modes most relevant to hydraulic control of the flow as a whole. Also relevant to interpretation of the data are the propagation characteristics of localized disturbances, which will be considered later.

#### 4. Stratification and flow

Lasting only one tidal cycle, the data groups are much too brief to estimate subtidal flow for comparison with long-term or seasonal averages. They are, however, adequate for understanding the striking contrasts in flow evolution and hydraulics observed during different years.

##### a. Subtidal

During 2001, average density decreased to landward below 20–25 m, as typical of estuaries, but the opposite was obtained at shallower depths (Fig. 6, top). Unlike many estuaries, Puget Sound has a major source of freshwater near its mouth, the Skagit River, entering on the east side of Whidbey Island. Some of this freshwater is advected around the southern end of the island into Admiralty Inlet near the mouth of Hood Canal.

Consistent with the along-channel density gradients, average currents across x1 flowed seaward above 20–30 m and landward below (Fig. 7). Peak speeds exceeded  $0.2 \text{ m s}^{-1}$  in both directions, and imposing a reasonable surface slope on the average density field produced geostrophic velocities similar to those observed. Average seaward flow at x2 (2001), across the sill crest, was strongly banked against the west side of the channel (not shown), but weak seaward flow was also observed above 25 m along the east side. Landward flow was centered slightly east of the thalweg. At x3 (2001), weak landward flow occupied half of the shelf east of the deep channel.

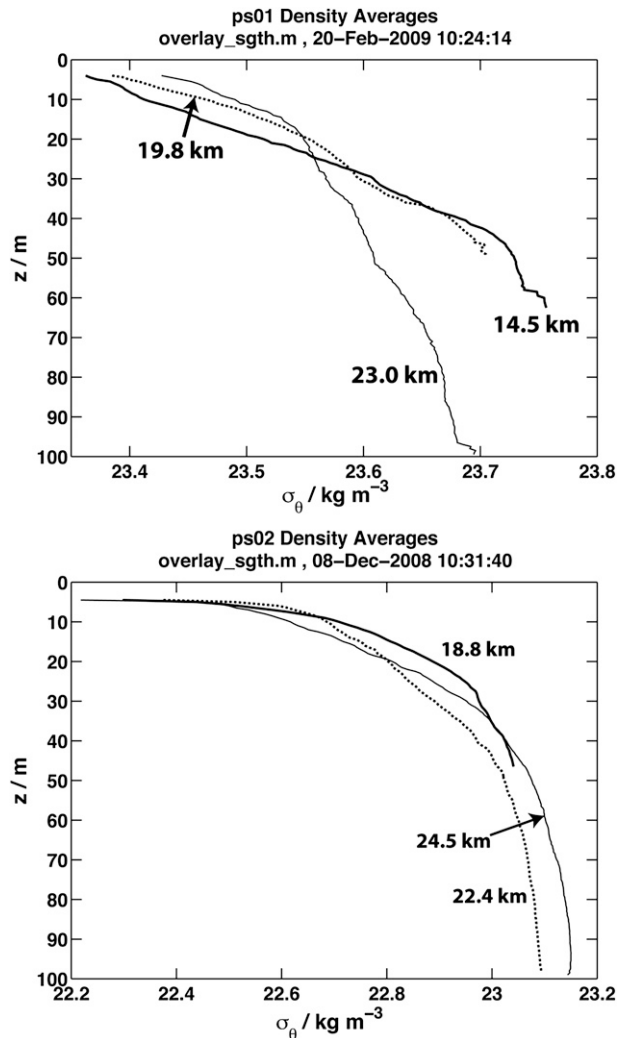


FIG. 6. Time-average  $\sigma_{\theta}$  profiles ( $\text{kg m}^{-3}$ ) along the thalweg across the sill during (top) th1 (2001) and (bottom) th3 (2002). During 2001, density increased to landward above  $z \approx 25$  m and decreased at greater depths. Most of the horizontal gradient was landward of the sill crest, at 19.8 km. During 2002, the situation was reversed. The decrease in  $\sigma_{\theta}$  was  $>0.5 \text{ kg m}^{-3}$  from 2001 to 2002.

The main flow, however, was in the deep channel landward of the hanging valley and extending upward along the west side to at least 20-m depth. Isopycnals shallower than 50 m rose toward the west, and the dense inflow had a potential density  $\sigma_{\theta} > 23.7 \text{ kg m}^{-3}$ . During 2001, landward transport was greatest for  $\sigma_{\theta} > 23.6 \text{ kg m}^{-3}$  (Fig. 8), with  $3.9 \times 10^3$  (x1),  $4.4 \times 10^3$  (x2), and  $2.0 \times 10^3 \text{ m}^3 \text{ s}^{-1}$  (x3). The lower value at x3 results at least in part from inadequate measurement of fast bottom currents with the vessel-mounted ADCP, but it is possible that dense water crossing x2 was mixed and did not reach x3. Missing the upper 5 m with the ADCP makes even larger underestimates of negative transports, by at

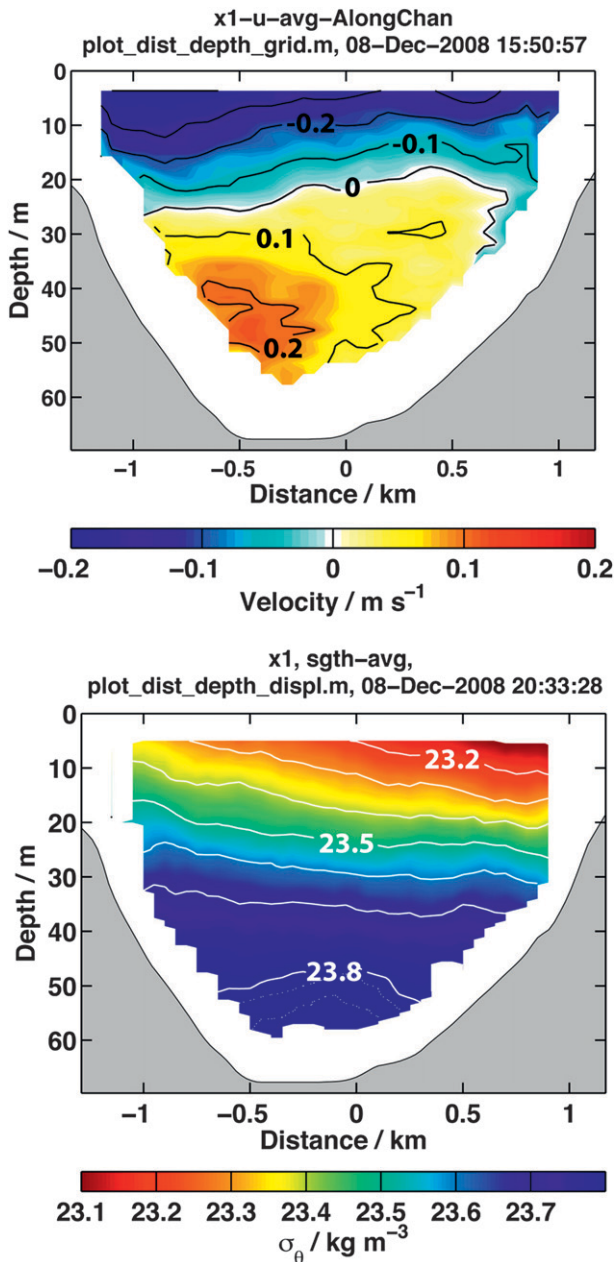


FIG. 7. Tidally averaged along-channel (top) velocity ( $\text{m s}^{-1}$ ) and (bottom)  $\sigma_\theta$  ( $\text{kg m}^{-3}$ ) on x1 (2001). Isopycnals tilted upward toward the west, and average flow was seaward shallower than  $z = 20\text{--}30$  m and landward below.

least  $0.2 \text{ m s}^{-1} \times 5 \text{ m} \times 2200 \text{ m} = 2.2 \times 10^3 \text{ m}^3 \text{ s}^{-1}$ . Because density increased to landward during 2002, there was negligible net flow across the sill, zero at x4 and only  $167 \text{ m}^3 \text{ s}^{-1}$  at x5 (2002), which was restricted to the upper 40 m along the west side.

The subtidal flow was strongly subcritical. For example, at the sill crest, solving (1) using stratification and velocity averaged across x2 (2001) yields speeds of 0.41,

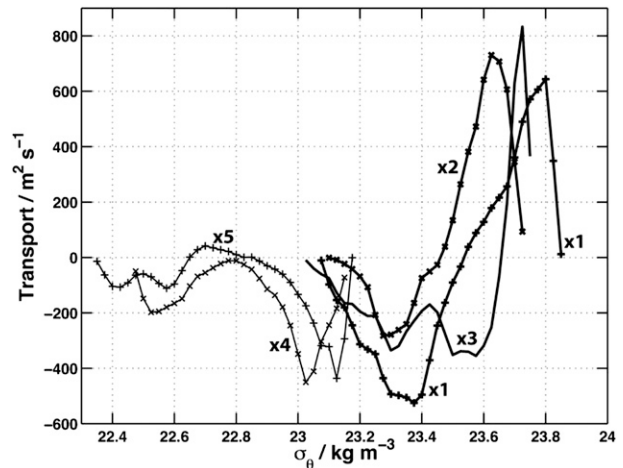


FIG. 8. Average along-channel transport ( $\text{m}^3 \text{ s}^{-1}$ ; positive landward) vs  $\sigma_\theta$  ( $\text{kg m}^{-3}$ ) for the five cross-channel tidal sections. There was a net flux of dense water,  $(2\text{--}4) \times 10^3 \text{ m}^3 \text{ s}^{-1}$ , across the sill during 2001 (x1, x2, and x3; thick lines) but not the next year (x4 and x5; thin lines), when only  $167 \text{ m}^3 \text{ s}^{-1}$  was observed.

0.19, and  $0.15 \text{ m s}^{-1}$  for internal modes 1, 2, and 3, respectively, compared to a mean speed of only  $0.04 \text{ m s}^{-1}$ .

### b. Tidal cycle

Average density differences along and across the channel dominated flow conditions around slack water, reversing currents at different times, depths, and places. For instance, along x2, the track along the sill crest sampled during 2001, at shallow depths flood began at slack tide in the eastern half of the channel while the same depths were still ebbing along x1. Deeper, near 30 m, all depths were flooding, but the flow was strongest in the east. Near the bottom, water was still ebbing on the west side.

More than 1 h before or after slack, tidal currents dominated the flow (Fig. 9). At peak ebb, deeper flows from landward followed the narrowing channel along the west side until redirected northeastward by the bend at the sill. The shallower flow diverged into the wider channel north of x3 (2001) but was mostly aligned with the main channel by x2 (2001). At peak flood, the deeper flow expanded laterally as it changed direction between x3 (2001) and x5 (2002). Above it, going south from x2, the constriction and sloping east side sharply deflected the flow toward the thalweg, apparently separating from the east side of the channel.

Consistent with the along-channel density gradient and the average transports it produced during 2001, tidal excursions were very asymmetric, producing net landward or seaward displacements for water deeper or shallower than approximately 30 m (Fig. 10, top). By the end of ebb, near-bottom water starting at x3 was 8 km to

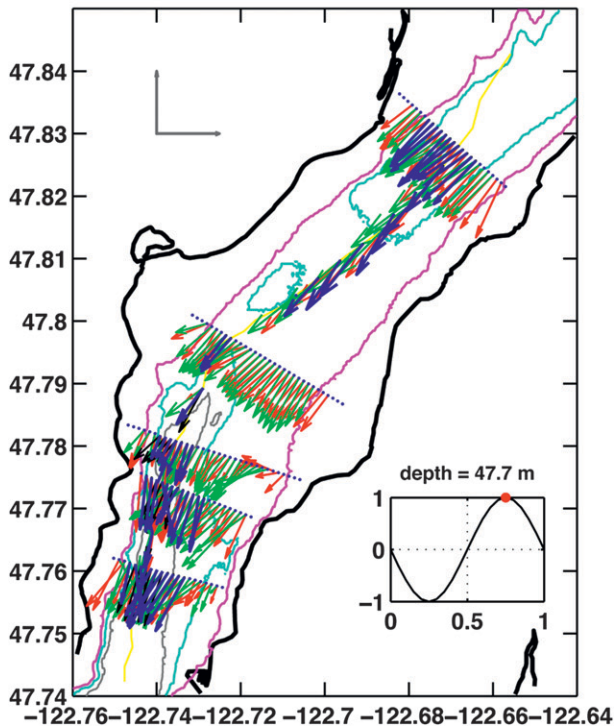
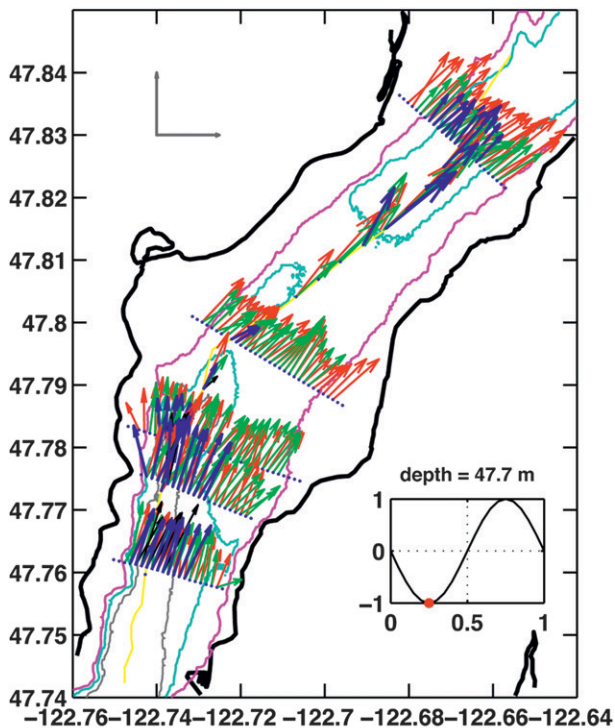


FIG. 9. Currents at (top) full ebb and (bottom) full flood interpolated from 2001 and 2002 observations. Vectors at 47.7 m (blue) are overlaid on others at 29.7 (green) and 11.7 m (red). Inserts show the tidal age as fractions of the cycle: 0.25 at peak ebb and 0.75 at peak flood. Reference vectors in the top left are each  $0.5 \text{ m s}^{-1}$ . Velocities from x1–x5 and th1 were used to make these plots.

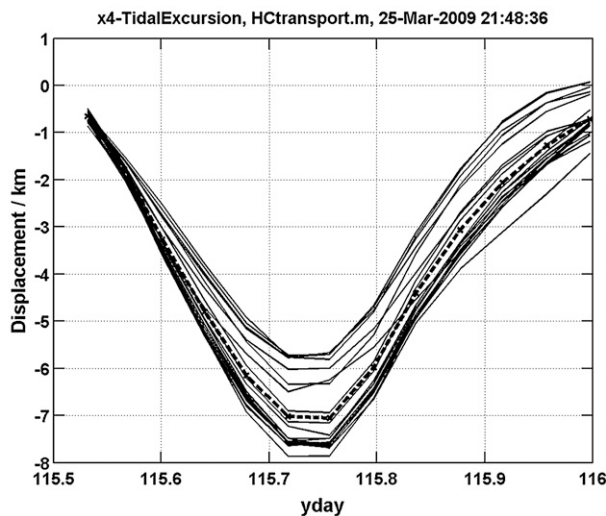
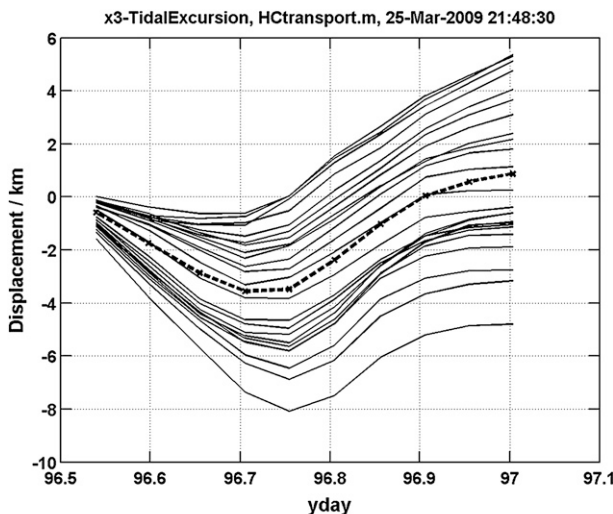


FIG. 10. Tidal excursions (km) of average along-channel velocities across (top) x3 during 2001 and (bottom) x4 during 2002, with shallow velocity bins at the bottom and deep ones at the top. Thick dashed lines are displacements of the section-average velocities. Although these sections were only 0.8 km apart, excursions during 2001 were very asymmetric, producing net motions strongly varying with depth, but those during 2002 were nearly symmetric, producing little net motion spanning less than 2 km.

seaward while near-surface water had moved less than 1 km. Stronger flood currents ended the cycle with deep water 5 km to landward and shallow water 5 km to seaward. Across x4 during 2002, displacements were nearly symmetric, ending the tidal cycle with shallow water approximately 1.5 km to seaward and deep water back where it started.

During 2001, dense water from x1 ended the tidal cycle 2–2.5 km to landward, halfway to the sill crest, thus requiring at least one more cycle to cross the sill (Fig. 10, top). Because the net displacement of water from the

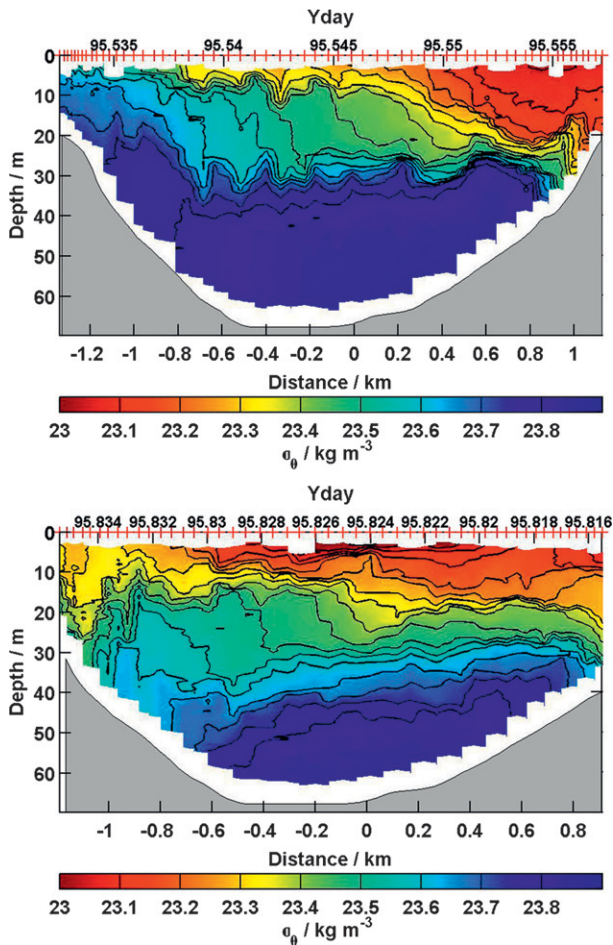


FIG. 11. Cross-channel  $\sigma_\theta$  oscillation along  $x_1$  (2001) during (top) peak ebb (sub 3) and (bottom) peak flood (sub 14). Red ticks at the top mark times (yearday) of profiles.

crest ( $x_2$ ) was 4 km (not shown), dense water starting the cycle there would not have returned but joined the large pool of dense water landward of the sill.

A strong cross-channel density oscillation accompanying the tidal cycle was most striking along  $x_1$  (2001), where the channel cross section is symmetric and the bottom is relatively smooth. During ebb, low-density water was concentrated and depressed along the east side while dense bottom water was pushed far up the west side (Fig. 11, top). During flood, the low-density water was spread farther across the channel and some was pushed down the west side (Fig. 11, bottom), creating overturns in some profiles. Dense bottom water was pushed downward along the west side, though it was only 10 m higher along the east side than during ebb. This pattern is consistent with forcing by Ekman transport at the bottom, analyzed in the Strait of Juan de Fuca by Martin et al. (2005); during ebb bottom Ekman transport was toward the west (Fig. 11, left), and during

flood it was toward the east. Consistent with this indication that the earth's rotation affects the flow, the internal Rossby radius of deformation at section  $x_1$  was 1.6, 0.6, and 0.4 km for baroclinic modes 1, 2, and 3, compared to a channel width of 2.4 km between 20-m isobaths [these were estimated by solving (1) for the actual stratification and channel width but no velocity to obtain speeds of  $c = 0.17, 0.067, \text{ and } 0.047 \text{ m s}^{-1}$ , yielding the Rossby radii as  $c/f$ , where  $f$  is the Coriolis parameter].

### c. Long waves and criticality

Wave speeds in 2001 at  $x_1$  (5 km seaward of the sill crest), at the crest itself ( $x_2$ ), and at the sill foot ( $x_3$ ; 2.1 km landward of the sill crest) are plotted over a tidal cycle (Fig. 12), with phase progressing along the vertical axis and short vertical lines marking  $c_{-1}, c_{-2}, c_{-3}, c_3, c_2,$  and  $c_1$ , from left to right. Solid curves are  $U_{\min}, U_{\text{avg}},$  and  $U_{\max}$ . All wave speeds are real and lie outside the range of the background velocity, as required by (4). In all cases, speeds for the third mode,  $c_{-3}$  and  $c_3$ , lie very close to  $U_{\min}$  and  $U_{\max}$ . At  $x_1$  and  $x_2$  (top and middle panels) the flows were strongly supercritical with respect to all three modes, becoming subcritical near slack tide. Because of the along-channel density gradient, ebb was faster than flood and lasted longer. Flow at  $x_3$  (bottom panel) was never supercritical during ebb, but it was critical for 1 h or more at peak flow. During flood tide, the first three modes were supercritical only during maximum flow, but the first mode remained supercritical for several hours before and after. Supercritical flow over such a long reach of channel, as well as over a substantial portion of the tidal cycle, is rather unusual.

During 2002, all three modes were strongly supercritical during most of flood and ebb at  $x_4$  and  $x_5$  (not shown), 1.0 and 2.5 km seaward of the steep sill base. This contrasts with the limited criticality of mode 1 found at the sill base during 2001, possibly because the deep flow there was underestimated as a consequence of side lobes masking near-bottom returns from the vessel-mounted ADCP.

“Local criticality” may also be defined for the flow at a given geographic location in a channel. Local criticality measures the ability of localized, hydrostatic waves to propagate upstream or downstream. These waves are long compared to the depth, but not the width, of the channel. Their troughs may be oriented at oblique angles to the channel axis. A shallow, homogeneous, free-surface flow with velocity components  $u$  and  $v$  is locally supercritical if the local Froude number  $F_r$  exceeds one [i.e., if  $F_r = (u^2 + v^2)^{1/2}/(gD)^{1/2} > 1$ ]. The flow can then support stationary “cross waves,” which have crests and troughs oriented at the angle  $\sin(F_r^{-1})$ . If the flow is

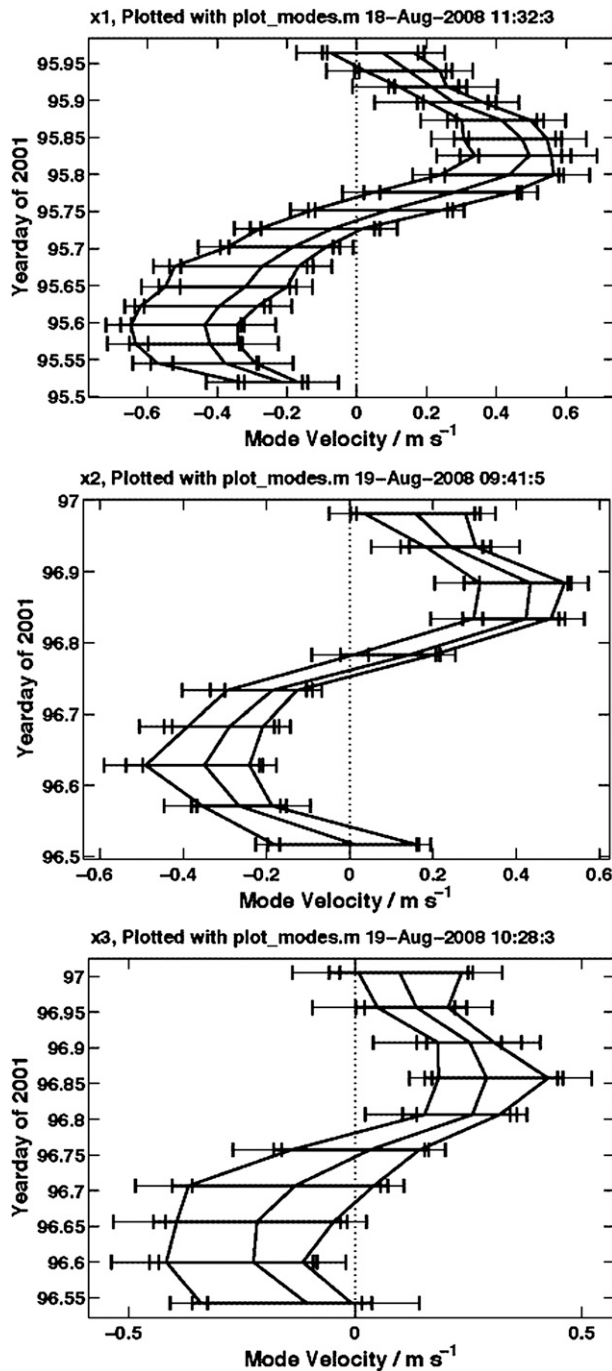


FIG. 12. Average water and mode velocities ( $\text{m s}^{-1}$ ) during 2001 across (top)–(bottom) x1 (14.9 km), x2 (20.0 km), and x3 (22.1 km). Curved vertical lines are cross-sectional averages of the minimum, average, and maximum flow speeds as time (yearday) increased along the y axis. The observations began after the start of ebb and concluded as flood was ending. Horizontal lines at average yearday for each crossing extend between the minimum and maximum baroclinic mode 1 speeds, marked by short vertical lines. The next pair of vertical lines going inward is the mode 2 speeds, and the innermost pair is the mode 3 speeds. A mode is supercritical when both of its speeds had the same sign.

locally subcritical [i.e., if  $(u^2 + v^2)^{1/2}/(gD)^{1/2} < 1$ ], stationary hydrostatic disturbances cannot exist. The complete theory for a homogeneous flow is summarized in Pratt and Whitehead (2008, section 4.3), and Winant et al. (1988) describe an atmospheric example, but there is apparently no generalization of this theory fitting Hood Canal conditions, in which the fluid is stratified and the velocity vector veers with depth. However, if we neglect this veering, we can estimate whether the flow at any horizontal location is locally subcritical or supercritical by solving (1) with  $T = 0$ , using the local profile of  $N^2$ , and  $U = (u^2 + v^2)^{1/2}$ . The local flow is then judged critical, supercritical, or subcritical with respect to mode  $j$  if  $c_j c_{-j} = 0, > 0$ , or  $< 0 \text{ m s}^{-1}$ , respectively.

### 1) 2001

Figure 13 compares the growth and decay of a hydraulic response downstream of the sill crest with estimates of local criticality during flood tide along the thalweg during section th1, and Fig. 14 (left) shows the along-channel velocity during sub 8. Each sub took slightly more than 1 h, starting at the landward end of the section in the top panel, which was run after flood was well established. Upstream of the crest, local accelerations and decelerations approaching the sill crest (Fig. 14, left) caused the flow to alternate between being slightly supercritical and almost critical. Over the steep landward sill face, however, the flow was definitely critical, turning strongly supercritical downstream. The densest water crossing the sill reached the bottom while intermediate densities were drawn down beneath a surface convergence, rebounding 1–2 km downstream. As flood slackened, flow became subcritical from the crest to its landward base, and the hydraulic response weakened. Upstream flow progressively lost supercritical regions and eventually was strongly subcritical, a sequence repeated later in the deeper water to landward. The hydraulic response was similar to hydraulic jumps and lee waves observed at sills with simpler bathymetry (e.g., Knight Inlet; Farmer and Armi 1999) but could also indicate cross waves (Pratt and Whitehead 2008).

Ebb tide during 2001 created a large, slowly moving “dome” of dense water that began on the seaward sill face, where the flow remained critical or subcritical throughout ebb, even at peak flow when everywhere else was strongly supercritical (Fig. 15). As it continued growing, the dome reached maximum thickness over the crest, tapering off several kilometers to seaward. Within the dome, flow varied from critical to supercritical, and by late ebb it had grown several more kilometers to seaward before tapering off. Runs across channel during x2 revealed that the dense water filled most of the channel, thinning west of the thalweg and beyond 1 km

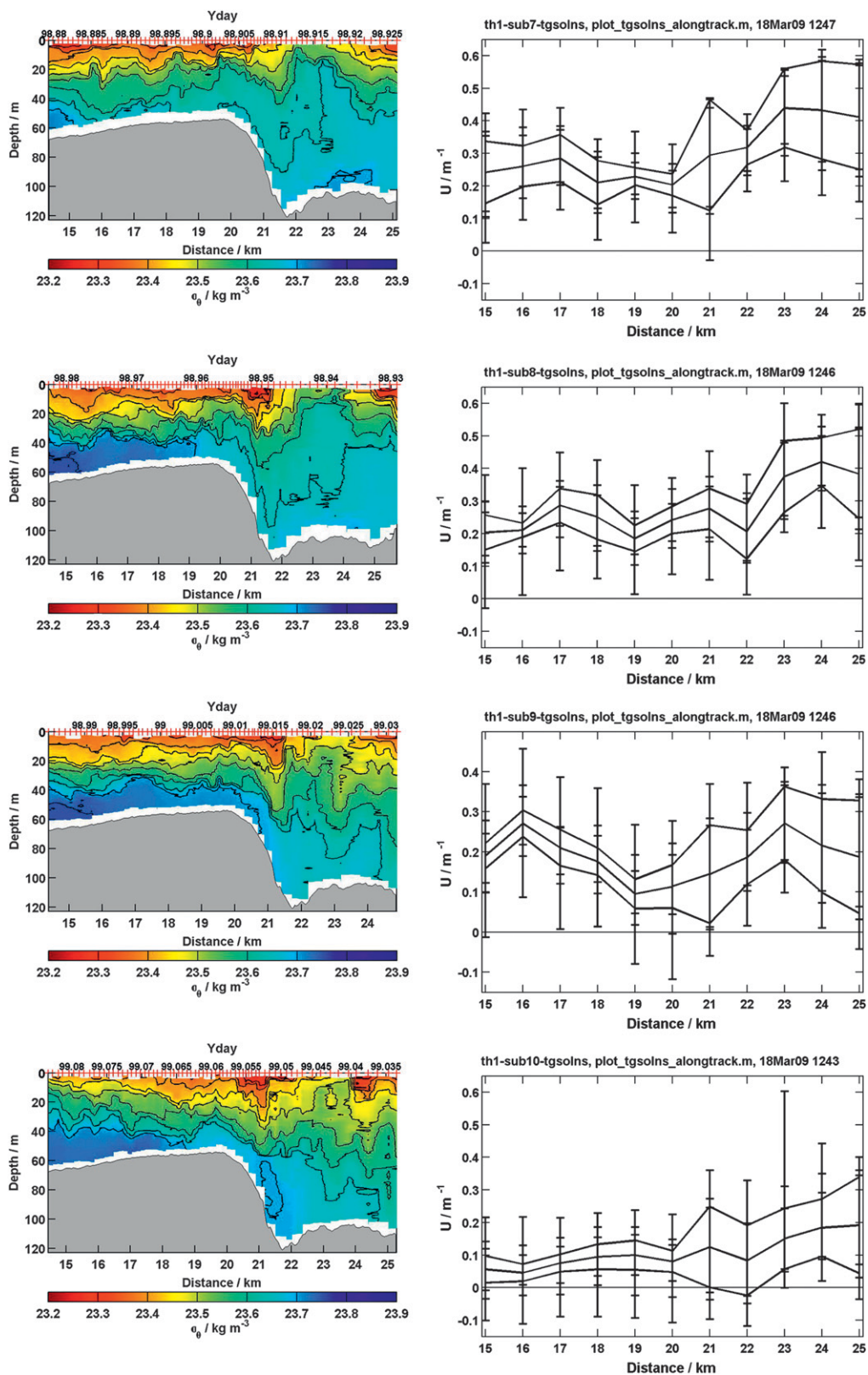


FIG. 13. The (left)  $\sigma_0$  (kg m<sup>-3</sup>) and (right) long-wave speeds (m s<sup>-1</sup>) along th1 (2001) during flood tide, with (top)–(bottom) subs 7, 8, 9, and 10.

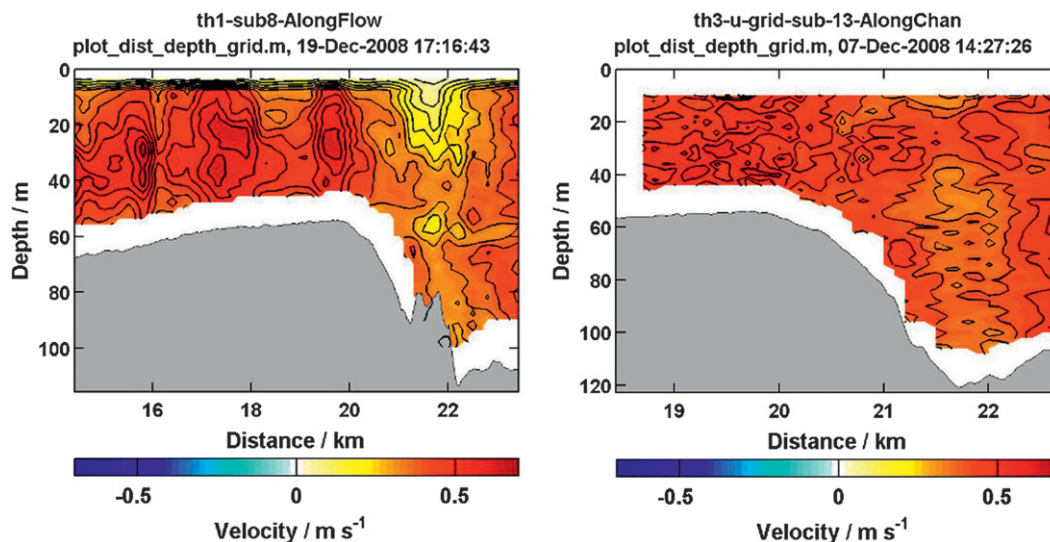


FIG. 14. Along-channel velocity ( $\text{m s}^{-1}$ ) near peak flood during (left) th1 (2001) and (right) th3 (2002). During 2001, the principal flow was forced below the sluggish water drawn down over the steep landward sill face. During 2002, the principal flow remained at middepth, passing over slower, with dense water beneath.

east of it, in both cases accompanied by displacements suggesting high-frequency waves. Similar short-wavelength features were also found in other cross sections. The dome bears some resemblance to the trapped pockets of dense air that can occur in the atmosphere when winds blow across valleys or depressions between hills (e.g., section 5.14 of Baines 1995). The hanging valley may provide the required depression. The Hood Canal dome differs from idealized atmosphere models by having dense fluid extending above the sill level and some distance downstream of the sill, instead of being confined to a valley. It is difficult, however, to extrapolate earlier work on isolated depressions or periodic hills and valleys to the present highly asymmetrical geometry.

## 2) 2002

In response to the change in along-channel stratification, ebb and flood evolved differently along the thalweg during 2002 than during 2001. Flow approaching the crest remained critical, or nearly so, even at maximum flood, and a small dome of dense water began 1 km upstream and extended down the sill face (Fig. 16). Water less dense than the dome passed over it and remained at middepth as the sill descended, unlike the situation during 2001 (Fig. 14, right). By the end of flood, the densest water had crossed the sill, forming an unstable dome 90 m high. Throughout most of flood, flow was supercritical past 22 km, strongly so at x4 (not shown).

During ebb, flow approaching the sill was strongly supercritical landward of 22 km, where it became critical (Fig. 17). Flow was at least briefly supercritical halfway up

the sill, at 21 km, but remained critical along the remainder of the section. A dome of dense water, similar to that observed the previous year, initially formed over the sill crest, but either it did not persist or it was so much larger that it tapered off seaward of our observations.

To observe evolution of flow bypassing the hanging valley, S1 was run along a streamline on the east side of the channel. Most notably, a large-amplitude wave formed during flood and persisted until it was nearly slack (Fig. 18). The upstream trough initially formed where control changed from strongly supercritical to critical, near 4 km along the S2 track, and gradually migrated upstream to 3 km as it deepened to reach the bottom. The control transition followed the trough upstream or possibly vice versa. A second trough formed 2 km downstream but remained shallower than the first trough. Because of its location and structure, the feature resembles a lee wave, but it may have been a cross wave, as discussed by Winant et al. (1988) and Pratt and Whitehead (2008).

## 3) 2003

Runs along S2 revealed a large wave (not shown) similar to that found the previous year along S2. The amplitude was not as large, but we cannot assess to what degree differences were due to location changes, contrasts in along-channel stratification, and somewhat stronger tides, as these measurements were taken late in the year when Earth is closer to the sun than it is during spring. The key finding, however, is that a large wave was observed nearby, demonstrating that the first observations were not unusual.

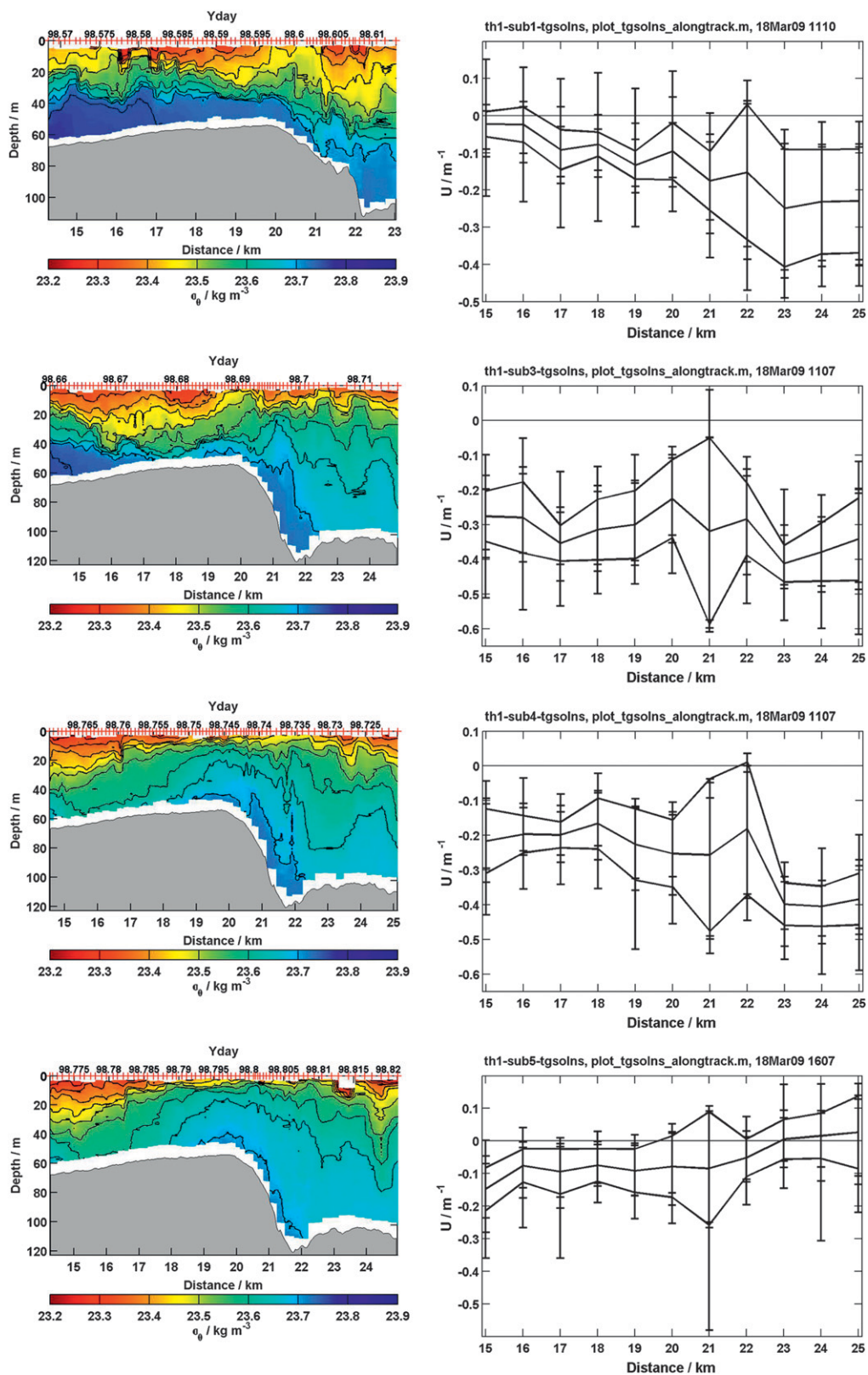


FIG. 15. As in Fig. 13, but during ebb tide, with (top)–(bottom) subs 1, 3, 4, and 5. Peak flow was critical on the steep sill face but supercritical upstream and downstream.

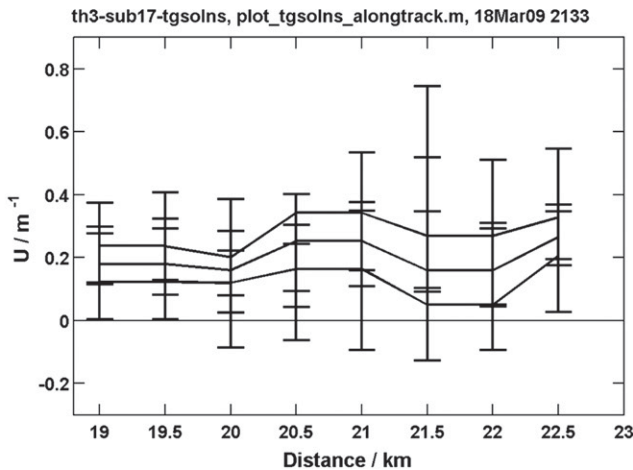
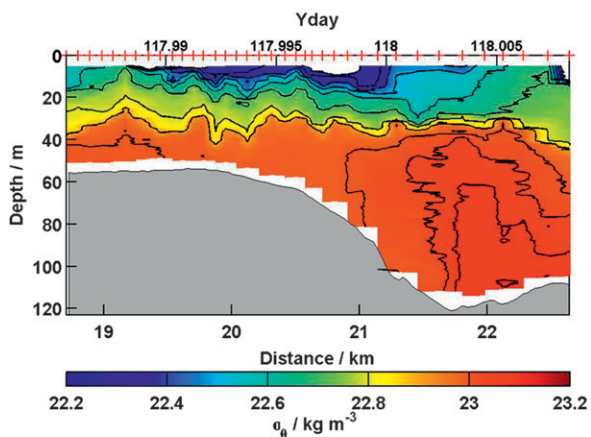
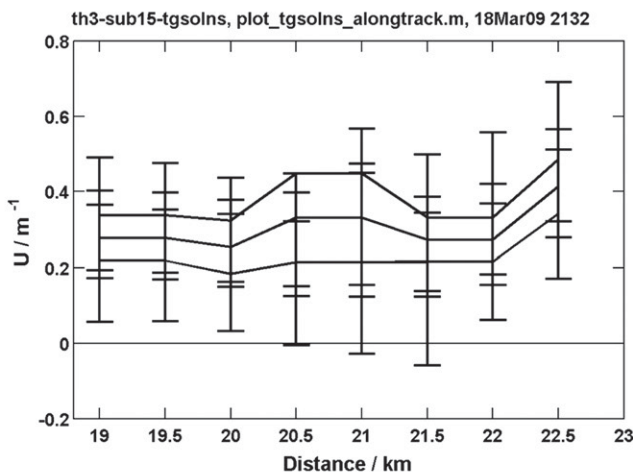
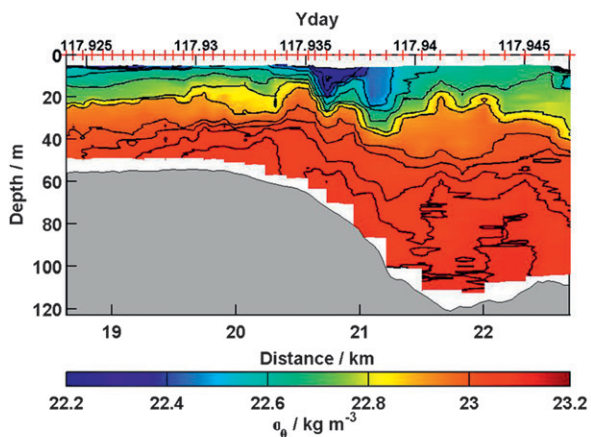
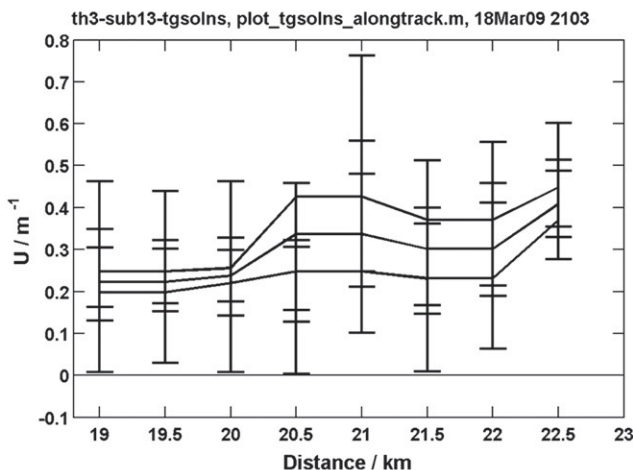
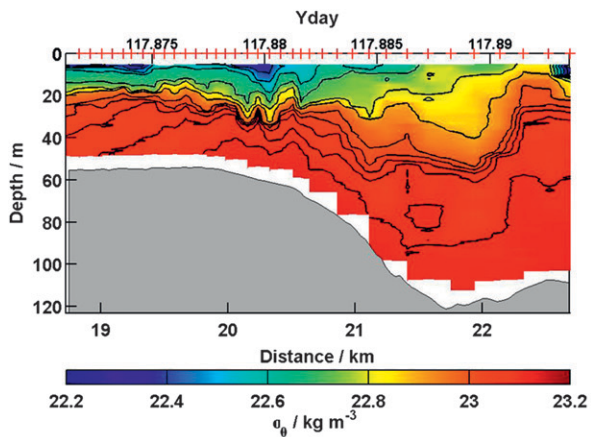


FIG. 16. The (left)  $\sigma_\theta$  ( $\text{kg m}^{-3}$ ) and (right) long-wave speeds ( $\text{m s}^{-1}$ ) along th3 (2002) during flood tide, with (top)–(bottom) subs 13, 15, and 17.

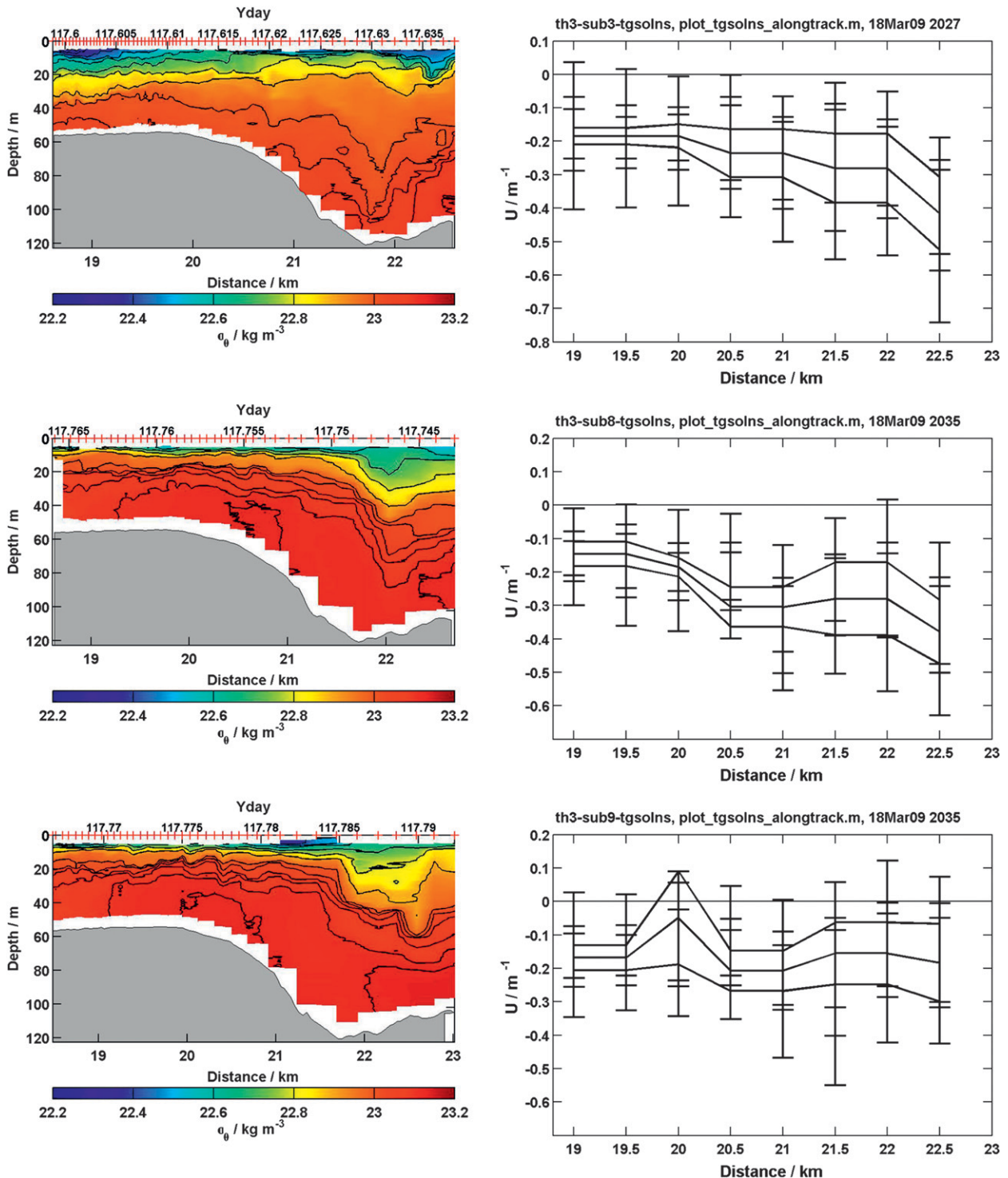


FIG. 17. As in Fig. 16, but during ebb tide, with (top)–(bottom) subs 3, 8, and 9.

Farther landward, the eight th4 transects along the thalweg (not shown) found flow slightly supercritical to mode 1 at 30 km during one run each near maximum ebb and flood. Several runs found mode 1 critical during

ebb, but during all the other transects it was subcritical, often strongly so. Modes 2 and 3, however, were supercritical during most of ebb and flood. Tidal variability was not adequately resolved near the ends of the line, as

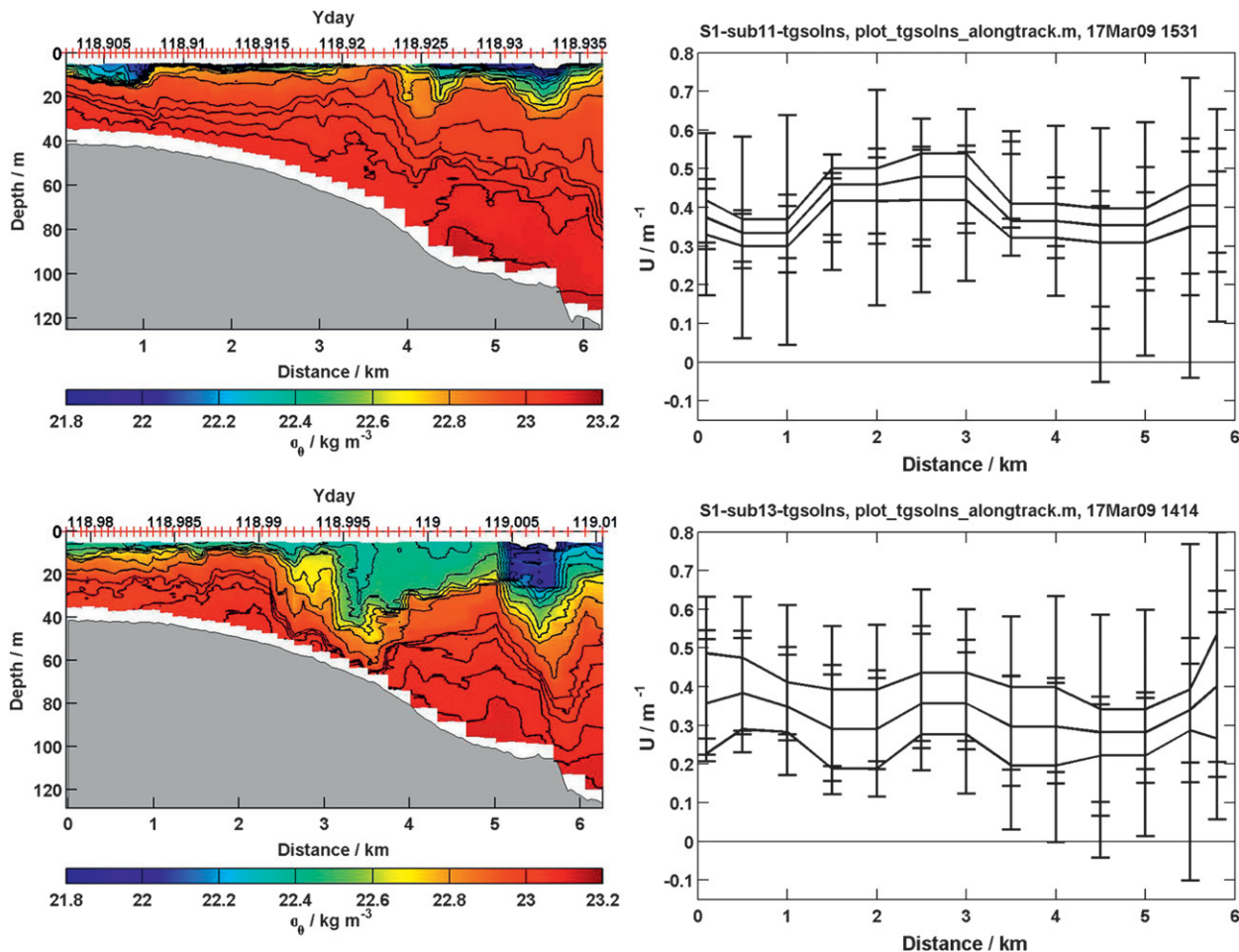


FIG. 18. Estimates of local criticality along S1 (2002) during (top) peak flood (sub 11) and (bottom) 1.8 h later (sub 13). Vertical lines span the propagation velocities ( $\text{m s}^{-1}$ ) of mode 1, with horizontal ticks for modes 1, 2, and 3. Curved horizontal lines mark maximum, average, and minimum average velocities along S1. Flow during sub 11 was either critical or barely supercritical upstream of 1 km, went strongly supercritical as the flow accelerated from 1 to 1.5 km, and did not return to critical until 4–4.5 km. During sub 13, the flow was supercritical until 3–3.5 km, where speeds slowed. In both cases, the flow appeared to return to being supercritical from 5.5 to 6 km, where it joined the flow along the thalweg.

back and forth visits were so close in time that they sampled nearly the same flow. With that caveat, we found mode 1 to be critical during peak flow at 26 km and always subcritical at 34 km. Concerned that the strongest flow may not be along the thalweg, we made one cross-channel run and found that to be the case but moderately so; consequently, the fastest flows may have been more supercritical than we observed. Nonetheless, we believe that in that region the flow was slowing and not as supercritical as found over and near the sill.

**5. Summary and discussion**

Although these observations provide unusual detail about spatial and temporal structure of hydraulic control, the complexities of bathymetry and flow exceed our

ability to understand fully the observations in terms of present theory. Bathymetric complexity includes multiple minima and maxima of cross-sectional area, with sill crest 4 km landward of the overall minimum and close to a maximum. In addition, the thalweg runs along the west side of the channel, forming a hanging valley at the sill crest. Aspects of common behavior include lee waves and density overflows, but often the familiar aspects are embedded in more complex behavior we do not understand; for example, Figs. 13–18 display behavior that is quite variable and difficult to classify according to conventional wisdom. These and other features have been described in some detail to stimulate future work, particularly on irregular channels and flows supercritical to internal waves. After summarizing the observations, we return to some of these themes.

During spring 2001:

- 1) Deep density decreased to landward across the sill, resulting in a subtidal exchange flow with currents exceeding  $0.2 \text{ m s}^{-1}$  and transport of  $2.0 \times 10^3 \text{ m}^3 \text{ s}^{-1}$  at the landward base of the sill. Above 25 m, along-channel density increased to landward, producing a mean seaward transport. After adding a reasonable cross-channel surface slope, geostrophic flows computed from the cross-channel tilt of tidally averaged isopycnals were similar to the observed exchange flow.
- 2) A strong cross-channel oscillation raised dense water 50 m above equilibrium depths along the west side during ebb and suppressed it during flood, while a similar oscillation having the opposite phase occurred along the east side of the channel. Amplitude and phase of the oscillation are similar to that observed in the Strait of Juan de Fuca by Martin et al. (2005), who demonstrate that the oscillation was forced by bottom Ekman layers. Significant rotation effects in a narrow channel are surprising, but deformation radii of internal modes 1, 2, and 3 are indeed less than the channel width.
- 3) When flood tide was well developed, flow was supercritical for modes 1 and higher for internal waves spanning the channel width at all three cross sections, x1 (5 km seaward of the crest), x2 (the crest), and x3 (the landward bottom of the sill). Before and after peak flood, control returned at x3 before it did at x1 and x2. Locally along the thalweg (th1), the flow varied from critical to slightly supercritical until the landward sill base, where it became strongly supercritical.
- 4) Supercritical approaching the sill, well-developed ebb flow was controlled at the sill base, returning to supercritical at the crest and seaward. As ebb developed, a large, sluggish dome of slow-moving dense water grew steadily over the sill. As ebb ended, the dome tapered toward the bottom seaward of the crest.

During spring 2002:

- 1) Density increased to landward across the sill, resulting in minimal subtidal exchange, cutting off any significant flow of dense water that we could observe.
- 2) Flood tide was critical approaching the sill and became supercritical in deeper water landward of the sill. Because of the denser water on the landward side, the strongest flow crossing the sill was at middepth.
- 3) Supercritical approaching the sill, ebb flow alternated between control and slightly subcritical to seaward. A dome formed again but was either more transient or so large that our track failed to reach its landward end.

- 4) Along streamline S1, along the gentle slope east of the thalweg, flood tide was supercritical or controlled at most times and places. Consequently, the large wave could not have been a traditional lee wave but was most likely a cross-channel wave, found where flows are supercritical.

During autumn 2003:

- 1) A large wave was observed along S2, smaller but otherwise similar to the one on S1.
- 2) Thalweg flow 6 and 8 km seaward of the sill base was locally supercritical for internal modes 1, 2, and 3 during most of ebb and flood.

On the flood tide, the density field can resemble an overflow with an internal hydraulic control at the sill and a hydraulic jump or lee wave regime landward (e.g., Fig. 13, top three rows; Fig. 16, top two rows). The long-wave speeds for these cases, however, suggest that the flow remains largely supercritical through the apparent jump or lee wave portion, suggesting that the observed disturbances could instead be cross waves. They could also be transients associated with the changing tide. The region upstream of the flow in these cases is not subcritical, as in standard overflows, but exhibits stretches of critical or supercritical flow. This suggests an alternative scenario, that of an approach control (Lawrence 1993; Zhu and Lawrence 1998) in which a control section exists upstream of a sill and the flow is supercritical over the sill itself. The region downstream of the sill in this case can experience a supercritical leap (a transition from a supercritical flow with a deep lower layer to another supercritical state with shallow lower layer); this does not, however, fit the observed density field.

The ebb produces many examples of flows that are supercritical between 22 and 26 km, which is consistent with the choke point in cross-sectional area at 31.5 km. In Figs. 15 (middle two rows) and 17 (middle row), this supercritical flow returns to a subcritical state at 21–22 km, in the vicinity of the hanging valley. The trapped dome of dense water is present here, and its presence may be associated with the recirculating roller in a hydraulic jump, just one of many interpretations.

It is apparent that each realization contains glimpses of familiar internal hydraulic behavior, but a complete explanation of any realization in terms of simpler, steady systems is difficult. One conclusion that is clear is that transitions between supercritical and subcritical flow are common and that hydraulic behavior is important in some general sense. Hydraulic transitions caused by topographic features are associated with blocking of the densest waters, and this may contribute to the hypoxic conditions that occur in the southern reach. Model studies

of stratified flows in a setting that is idealized but contains some of the geometrical complexity and time dependence of Hood Canal are required.

The subtidal flow resembles a weak estuary circulation that exists in the presence of strong tidal fluctuations. A picture of how the fluctuations might alter the mean is provided by Helfrich (1995), who studied two-layer exchange in the presence of barotropic fluctuations. He explores several geometries, and the one most relevant to Hood Canal has a sill separated from a narrows by a length  $L$ . The outcome is then largely a function of two parameters, the first being the ratio  $\gamma = cT/L$  of the distance that an internal wave with speed  $c$  travels over one tidal period  $T$  to the separation scale  $L$ . In Hood Canal, we identify the cross-sectional area minimum (at 15.5 km) and sill (at 20 km) as reasonably corresponding to this narrows and sill, so  $L \approx 5$  km. The value of  $c$  in Helfrich's two-layer system is a wave speed scale  $(g'D)^{1/2}$  based on the resting stratification. For  $c$ , we can use the speed for mode  $j$  given by the eigenvalue of the extended Taylor–Goldstein equation for a rest state, approximately  $0.5 \text{ m s}^{-1}$  for mode 1. With  $T \approx 12$  h, these settings lead to  $\gamma \approx 4$ , with smaller values for higher modes. Helfrich finds that the strongest enhancement of the two-layer exchange by the fluctuating barotropic tide occurs when  $\gamma$  is very large. This is the quasi-steady limit explored by Armi and Farmer (1986), in which the flow can be considered dynamically steady at a given instant. Helfrich finds that  $\gamma$  needs to be on the order 30 for this limit to be reached, and the Hood Canal time dependence by this measure must be considered rapid.

The second parameter is Helfrich's  $q_{b0}$ , which is the ratio of the barotropic tidal velocity to  $c$ . For the first vertical mode, the parameter is similar to  $ND/\pi U$ , which was given in section 3 to be approximately 0.6. Moreover, the extended Taylor–Goldstein analysis revealed that the flow is critical or reasonably close to critical over long stretches of the channel during a significant portion of the tidal cycle, confirming that  $q_{b0} = O(1)$  for mode 1. For  $\gamma = 4$  and  $q_{b0}$  in the range 0.6–1, the time dependence leads to a modest amplification of the exchange flow of 1.3–1.5 (see Helfrich's Fig. 9); that is, mean exchange flow is 1.3–1.5 times larger in magnitude than what it would be without tides. Coincidentally, these are the exact parameter values that he uses for a numerical experiment shown in his Fig. 10. During the equivalent of the Hood Canal ebb tide, the lower layer becomes very thin and nearly disappears landward of the sill. One caveat to the overall comparison is that the initial, steady exchange flow that is perturbed in Helfrich's model is maximally controlled. A correspondence between Hood Canal and that initial state is not clear. Another caveat is that the exchange may be reduced by friction, even

below the steady level. This is shown by Li and Lawrence (2009), though in a contraction-only geometry difficult to relate to the present setting.

*Acknowledgments.* Washington State Sea Grant funded collection of these observations and the Office of Naval Research their publication. Pratt's efforts were supported by the National Science Foundation under Grant OCE-0525729. Jack Miller, Dave Winkel, Steve Bayer, Earl Krause, and Andrew Cookson prepared the instruments, participated in data collection, and helped during analysis. Eric Boget skillfully and diligently operated the R/V *Miller*, sometimes in difficult circumstances. By letting us work in base waters, numerous officers from the U.S. Naval Submarine Base Bangor made possible key parts of our surveys and facilitated our access to base waters. Parker MacCready offered valuable comments.

## REFERENCES

- Armi, L., and D. M. Farmer, 1986: Maximal two-layer exchange through a contraction with barotropic net flow. *J. Fluid Mech.*, **164**, 27–51.
- Baines, P., 1995: *Topographic Effects in Stratified Flows*. 1st ed. Cambridge University Press, 482 pp.
- Deng, J., L. Pratt, L. Howard, and C. Jones, 2003: On stratified shear flow in sea straits of arbitrary cross section. *Stud. Appl. Math.*, **111**, 409–434.
- Farmer, D., and L. Armi, 1999: Stratified flow over topography: The role of small scale entrainment and mixing in flow establishment. *Proc. Roy. Soc. London*, **455A**, 3221–3258.
- Helfrich, K. R., 1995: Time-dependent two-layer hydraulic exchange flows. *J. Phys. Oceanogr.*, **25**, 359–373.
- Lawrence, G. A., 1993: The hydraulics of steady two-layer flow over a fixed obstacle. *J. Fluid Mech.*, **254**, 605–633.
- Li, S., and G. Lawrence, 2009: Unsteady two-layer hydraulic exchange flows with friction. *J. Fluid Mech.*, **633**, 99–114.
- Martin, W., P. MacCready, and R. Dewey, 2005: Boundary layer forcing of a semidiurnal, cross-channel seiche. *J. Phys. Oceanogr.*, **35**, 1518–1537.
- Newton, J., A. Devol, M. Kawase, W. Ruef, M. Warner, D. Hannafious, and R. Rose, 2007: Hypoxia in Hood Canal: An overview of status and contributing factors. *Proc. Georgia Basin Puget Sound Research Conf.*, Seattle, WA, University of Washington School of Engineering, 10 pp. [Available online at [http://www.engr.washington.edu/epp/psgb/2007proceedings/papers/9a\\_newton\\_comp.pdf](http://www.engr.washington.edu/epp/psgb/2007proceedings/papers/9a_newton_comp.pdf).]
- Pratt, L. J., and J. A. Whitehead, 2008: *Rotating Hydraulics*. Springer, 589 pp.
- , H. E. Deese, S. P. Murray, and W. Johns, 2000: Continuous dynamical modes in straits having arbitrary cross sections, with applications to the Bab al Mandab. *J. Phys. Oceanogr.*, **30**, 2515–2534.
- Winant, C., C. Dorman, C. Friehe, and R. Beardsley, 1988: The marine layer off Northern California: An example of supercritical channel flow. *J. Atmos. Sci.*, **45**, 3588–3606.
- Winters, K., and J. Riley, 1992: Instability of internal waves near a critical level. *Dyn. Atmos. Oceans*, **16**, 249–278.
- Zhu, D., and G. Lawrence, 1998: Nonhydrostatic effects in layered shallow water flows. *J. Fluid Mech.*, **355**, 1–16.